NOS and SONOS redox switches in proteins

Fabian Rabe von Pappenheim
University Goettingen https://orcid.org/0000-0002-3925-8127
Marie Wensien
University Goettingen
Jin Ye
University Goettingen
Jon Uranga
University Goettingen https://orcid.org/0000-0002-1256-6656
Lisa-Marie Funk
University Goettingen
Ricardo Mata
University Goettingen
Kai Tittmann (Kai.Tittmann@biologie.uni-goettingen.de)
University Goettingen https://orcid.org/0000-0001-7891-7108

Article

Keywords: Lysine-cysteine Redox Switch, Native Branching Crosslink in Proteins, Enzyme Catalysis, Binding of Substrates

Posted Date: July 2nd, 2021

DOI: https://doi.org/10.21203/rs.3.rs-635771/v1

Version of Record: A version of this preprint was published at Nature Chemical Biology on February 14th, 2022. See the published version at https://doi.org/10.1038/s41589-021-00966-5.

NOS and SONOS redox switches in proteins

Fabian Rabe von Pappenheim [1,2], Marie Wensien [1,2], Jin Ye [3], Jon Uranga [3], Lisa-Marie Funk [1,2], Ricardo A. Mata [3], & Kai Tittmann [1,2 *]

[1] Department of Molecular Enzymology, Göttingen Center of Molecular Biosciences, Georg-August University Göttingen, Julia-Lermontowa-Weg 3, D-37077 Göttingen, Germany

[2] Department of Structural Dynamics, Max-Planck-Institute for Biophysical Chemistry, Am Fassberg 11, D-37077 Göttingen, Germany

[3] Institute of Physical Chemistry, Georg-August University Göttingen, Tammannstraße 6, D-37077 Göttingen, Germany

[*] To whom correspondence shall be addressed: ktittma@gwdg.de (K.T.)

We recently reported on the discovery of a lysine-cysteine redox switch in proteins with a covalent NOS bridge. Here, a systematic survey of the whole protein structure database discloses that NOS bridges are ubiquitous, hitherto overlooked redox switches in proteins of all domains of life and are found in diverse structural motifs and chemical variants. In several instances, lysines are observed in simultaneous linkage with two cysteines forming a SONOS bridge with a trivalent nitrogen, which constitutes the first native branching crosslink in proteins. In many proteins, the NOS switch contains a functionally essential lysine with direct roles in enzyme catalysis or binding of substrates, DNA or effectors linking lysine chemistry and redox biology as a novel regulatory principle. The NOS/SONOS switches are frequently found in proteins from human and plant pathogens including i.a. SARS-CoV-2 but also in many human proteins with established roles in gene expression, redox signaling and homeostasis in both physiological and pathophysiological conditions. Targeting, mimicking, controlling and engineering the NOS and SONOS redox switches appear to open novel avenues in drug, antiviral, antibiotic and herbicide development, in biocatalytic applications as well as in protein design and bioorganic chemistry.

Introduction

Reactive oxygen species (ROS) are central to redox signaling in all domains of life and critically control cell growth, development, metabolism, aging and the response to stress conditions as e.g. infection by pathogens [1-4]. At elevated levels, ROS induce oxidative stress that has been implicated in a myriad of pathologies including cancer, neurodegenerative diseases, inflammation and autoimmune conditions [5,6]. The underlying molecular mechanisms of redox signaling and oxidative stress have been mostly attributed to chemical modifications of cysteine residues in redox-sensitive proteins with key reactions being disulfide bridge formation between two cysteines or oxidation, glutathionylation and nitrosylation of individual cysteines [7,8]. We have recently reported the discovery of an allosteric lysine-cysteine redox switch with a covalent NOS bridge that regulates the enzymatic activity in response to changing redox conditions [9]. Here, we systematically mine the available protein structure database for proteins with undetected lysine-cysteine redox switches and find hitherto unidentified NOS bridges in proteins from all domains of life with critical roles in central cellular functions including metabolism, gene expression, signaling,

the ubiquitin pathway, DNA repair and redox homeostasis. These findings bear wide-ranging biological implications in the context of redox signaling, oxidative stress and many human disease states.

Results and Discussion

Geometric properties of NOS bridges

Before we analyzed the deposited experimental protein structures in the protein database (www.rcsb.org) to search for potentially undetected covalent NOS bridges, we set out to define the geometric properties of these versus non-covalent H-bond interactions between cysteine and lysine residues to identify reliable criteria to discern between these scenarios. A survey of H-bond interactions of cysteines in protein structures disclosed mean interatomic S-N distances of 3.44 Å with lysine residues (cysteine as acceptor) and 3.75 Å for the case when cysteine acts as H-bond donor [10]. However, the closest possible physical encounter between the two side chains remained to be defined. To close this gap of knowledge, we conducted quantum chemical calculations, where we analyzed the geometric properties of i) the NOS bridge, ii) a hydrogen bond between lysine as amine ($-NH_2$) and cysteine (-SH) and iii) a hydrogen bond between protonated lysine ($-NH_3^+$) and cysteine (-SH). An extensive conformational search was performed for the two residues in all three scenarios at different α-carbon atom distances (ED Fig. 1). Several theoretical methods (also considering different dielectric constants, SI Fig. 1) provided a consistent picture, whereby all minima featuring an N-S distance below 3.1 Å exhibited a covalent NOS bridge. The covalently bound NOS conformers displayed a bimodal distribution of the N-S 1,3 distance, with two maxima in the 2.6-2.7 Å range. This is a purely steric effect resulting from the relative positioning of the sulfur atom to the lysine chain (SI Fig. 2). Hydrogen-bonded lysine-cysteine pairs are formed at much larger distances, with minimal values hovering at 3.2 Å for a protonated lysine-cysteine interaction, increasing to 3.5 Å once a proton is removed. The computational results signal a clear difference between the three types of interactions, with the lowest energy distributions showing no overlap. The results are also consistent independent of the relative positioning of the two residues.

Detectability of NOS bridges in crystallographic protein structures

Next, we tested the impact of resolution and deposited dose in X-ray crystallographic experiments on the traceability of covalent NOS bridges in protein structures (ED Fig. 2). We had initially detected the NOS redox switch in protein crystals that diffracted beyond 1 Å, a resolution that is rarely accomplished in protein crystallography but is required to unambiguously define the chemical nature of atoms and their connectivities [11]. We used a sub-ångstrøm dataset obtained for one of these crystals and truncated the diffraction data at 1.0, 1.5, 2.0, 2.5 and 3.0 Å, and further omitted the bridging oxygen atom of the NOS bridge for structure refinements to eliminate model bias (ED Fig. 2a). As one would expect, the detectability of the covalent crosslink is critically dependent on the resolution: while the presence of the bridging atom is verifiable up to resolutions of 2 Å based on both the 2mFo-DFc as well as mFo-DFc difference electron density maps, the interpretation of electron density maps at lower resolutions becomes ambiguous. In the transaldolase protein crystals we analyzed, the NOS bridge exhibits almost full occupancy and our system may therefore be regarded as a best-case scenario (also considering the low B-factors). To test the impact of high-energy synchrotron radiation on the NOS bridge in protein crystals, which is known to promote “radiation damage” of redox-sensitive groups [12], we conducted dose-dependent experiments depositing calibrated doses between 0.5 and 10 MGy in 0.5 MGy increments (ED Fig. 2b, X-ray crystallographic statistics in SI Table 1). These experiments reveal that the NOS bridge in the tested protein crystals is relatively robust and withstands doses up to 5 MGy, where radiation damage at neighboring acidic side chains becomes visible. Only when we deposited high doses of 10 MGy, we detected a slight decomposition of the NOS bridge. In sum, to reliably detect NOS bridges in protein crystal structures, a resolution of better than 2 Å is required as well as a high occupancy of this group and sufficient local order. “Radiation damage” can be excluded to cause NOS bridge formation artificially as we have demonstrated before [9], to the contrary, NOS bridges decompose while interacting with high-energy radiation but only at very high doses.

On the basis of the quantum chemical calculations and the X-ray crystallographic experiments on our model system, we downloaded all pdb entries with a resolution of ≤2 Å (65 000) including the corresponding structure factors and electron density

maps, if available. We then searched for close contacts between lysine and cysteine residues, specifically pairs with interatomic N-S distances of less than 3 Å, which are in the regime of covalent NOS bridges rather than H-bond interactions (>3.2 Å). We identified 266 deposited structures with ~400 potential NOS bridges (SI Data 1), and manually inspected the putative lysine-cysteine crosslink site in all these structures. In almost all deposited structures, the corresponding lysine and cysteine residues were built without a crosslink, in very few with a methylene bridge and in one except our own structures with an NOS link. We remodeled both residues with a covalent crosslink, either as an NOS bridge, or, alternatively, as a direct N-S linkage (sulfenamide) using geometrically parametrized restraints. We consider formation of a methylene (N-CH_2-S) bridge as highly unlikely as previously discussed by us and others [9,13]. We then re-refined the structures and compared the obtained models and electron density maps for the three alternative scenarios: i) a covalent NOS linkage, ii) a covalent N-S linkage and iii) a non-covalent H-bond interaction (as deposited). In ~150 data sets, the existence of an NOS bridge is highly likely (~100) or possible (~50), while a non-covalent H-bonding interaction or direct N-S linkage can be relegated in these data sets to minor probability (SI Data 1). In a few datasets, the electron density maps clearly indicate the presence of a crosslink but the quality is insufficient to discriminate between a NOS bridge and a direct N-S bond (sulfenamide). Proteins from human or plant pathogens (ED Table 1) and human proteins (ED Table 2) are summarized individually.

Structural and chemical motifs of NOS bridges

NOS bridges are observed in an amazing diversity of structural motifs and chemical variations (Fig. 1, Fig. 2). First, we analysed the distance distribution in sequence between the NOS bridge lysine and cysteine residues –Cys^{a}–$(X)_{n-1}$–Lys^{a+n}–, where a and a+n denote the corresponding sequence positions and n the sequence distance (Fig. 2a). This analysis reveals a Gauss-like distribution with the largest fraction of NOS bridges observed for short sequence distances (n <|10|) and the smallest distance being two positions in sequence (n+2) in intra-strand/strand-like structures (Fig. 2b). Other motifs include intra-helical NOS bridges (mostly n+4) (Fig. 2c), inter-strand bridges in e.g. barrel structures (Fig. 2d), bridges connecting helices and strands (Fig. 2e), or intra-loop bridges (Fig. 2f). Most NOS bridges are formed intramolecularly within one protein chain, in a few examples we detected

intermolecular crosslinks, either as single bridges between two different proteins (A-B type) or as an NOS "double bridge" in homodimeric assemblies (A_2-type), where the corresponding lysine and cysteine residues of each chain form two reciprocal NOS bridges (Fig.1, Fig. 2g). In one case, an NOS bridge is observed for a cysteine that is alternatively engaged in a disulfide bridge suggesting a "mixed" disulfide-NOS redox switch site (Fig. 2i). In terms of the oxidation state of the NOS cysteine, we exclusively found mono-oxidized species (sulfenic acid equivalent), there is not a single case where the cysteine sulfur is in a higher oxidation state (bonded to more than one oxygen atom). However, we discovered that in some proteins lysines may form NOS bridges with two cysteines at the same time constituting a branching SONOS bridge, in which the lysine nitrogen is in a di-oxidized nitro-state as shown for e.g. galectin-1, a redox-sensitive protein with numerous important biological functions [14] (Fig. 1, Fig. 2h, ED Table 2). To the best of our knowledge, the SONOS group would be the first native branching crosslink between amino acids in proteins. Amino-acid derived redox cofactors, which are formed through crosslinks between two and in rare cases three amino acids (e.g. Met-Tyr-Trp) do not possess a single branching center as the lysine nitrogen atom of the SONOS group [15,16]. Other examples for proteins with SONOS bridges include the main protease (Mpro) from SARS-CoV-2 (Fig. 3), an important drug target for fighting the current COVID-19 pandemic [17,18], and the human Nsf1-IscU complex that is central to the Fe-S cluster biogenesis in mitochondria [19] (ED Fig. 3). In both cases, structures with either an NOS or a SONOS bridge of the same redox switch were detected suggesting a stepwise oxidation (Fig. 1). While the initial oxidation (NOS) involved structurally proximal lysine and cysteine residues, the second oxidation (SONOS) involved in both cases a 'mobile' cysteine that structurally fluctuates between the active sites and the redox site (Fig. 3, ED Fig. 3).

Catalytic requirements for NOS/SONOS bridge formation

In our initial discovery of the allosteric NOS redox switch in the enzyme transaldolase from *Neisseria gonorrhoeae* [9], we had speculated that a neighboring glutamate (Glu93) might be catalytically essential for formation of the NOS bridge akin to the suggested role of a glutamate in isopeptide bond formation in some proteins [20] (ED Fig. 4a). However, in many proteins with identified NOS or SONOS bridges, no amino acid capable of acid-base catalysis is found in the immediate

vicinity of the redox switch pinpointing to an intrinsic reactivity of structurally proximal lysine and cysteine residues provided ROS and/or O_2 are present. To test this hypothesis, we generated a transaldolase Glu93Gln variant, in which a potential catalytic role of residue 93 is eliminated, and analysed the structure and enzymatic properties of the variant. The kinetic constants are very similar to the wild-type enzyme except for a slight 1.5-fold increase in the substrate Michaelis constant (SI Table 2), and the variant remains redox activatable. The structural analysis of the Glu93Gln variant by X-ray crystallography (SI Table 1) clearly indicates formation of the NOS bridge argueing against a compulsory catalytic mode involving a neighboring amino acid (ED Fig. 4b). This mechanistic proposal is also supported by the finding that a lysine-cysteine crosslink was unintentionally engineered into the penicillin-binding protein 4 from *Staphylococcus aureus*, where the catalytic nucleophile Ser95 at the active site had been replaced by a cysteine that forms a crosslink with the co-catalytic Lys98 (ED Fig. 4c-e). Likewise, a positional inversion of the NOS-bridge forming lysine and cysteine residues in the human DNA repair enzyme OGG1 resulted in the formation of an NOS bridge akin to the wild-type configuration (ED Fig. 4f-i). While amino acid or enzyme catalyst are not compulsory for NOS bridge formation in vitro, we cannot exclude enzyme or metal ion catalysis under in vivo conditions as in case of disulfide bonds [21].

Chemical functions of the NOS lysine and cysteine residues

In a next step, we analyzed the chemical functions of the lysine and cysteine residues forming the NOS/SONOS redox switches in the context of the respective protein structure and function. In the previously reported redox-sensitive transaldolase, the NOS bridge functions as an allosteric switch that changes the structure of the protein including that of the active site, and thereby regulates enzymatic activity [9]. The operational modes of the NOS/ SONOS redox switch residues in the now identified proteins are amazingly diverse and can be classified into several major classes including lysines with direct catalytic roles, lysines with direct binding roles, cysteines with direct catalytic roles, and allosteric switches (Fig. 4, Fig. 5). The manifold chemical tasks associated with the NOS lysine residues are particularly intriguing and include the full spectrum of lysine roles in protein function. NOS bridges were identified for proteins with catalytic lysines that form i) Schiff-bases with the PLP cofactor in PLP-dependent enzymes (e.g. arginine/ornithine

decarboxylase), ii) Schiff-bases with enzymatic substrates (e.g. KDPG aldolase), iii) carbamate intermediates in covalent CO_2 transfer to biotin (e.g. oxaloacetate decarboxylase/Na^+ pump) and lysines that iv) act as acid-base catalysts in the active site of enzymes (e.g. penicillin binding protein) (Fig. 4a-d). Apart from these catalytic roles, numerous proteins were identified, where the NOS lysine is directly involved in binding of enzymatic substrates (e.g. DAH7P synthase) or of effectors as e.g. inositolphosphates (e.g. rabphilin), often interacting with a negatively charged moiety of substrate or effector (Fig. 4e-f). In other cases, the NOS bridge is located proximal to regulatory metal binding sites (e.g. Ca^{2+}) (Fig. 4f-g). An interesting observation concerns the involvement of the NOS bridge lysines in direct binding of DNA. In e.g. DNA polymerase, the lysine interacts with the base moiety of single stranded DNA (Fig. 6a), while in homeobox protein Hox, it binds to the phosphate backbone of double stranded DNA (Fig. 6b). Interestingly, NOS redox switches are also found for histone writers and erasers suggesting a critical and multilayered role of these switches for the regulation of gene expression (Fig. 6c,d). Catalytic cysteines were detected for several ubiquitin E2 ligases (ED Fig. 5) and the FeS cluster biogenesis complex Iscu-Nsf1 (ED Fig. 3) as discussed before. It seems reasonable to suggest that under oxidizing conditions (e.g. oxidative stress by ROS) formation of NOS/SONOS bridges in proteins, where the lysine and cysteine residues have direct roles in catalysis, goes along with a (reversible) loss of function. In case of direct roles in the binding of enzymatic substrates, effectors or DNA, NOS bridge formation would lead to a reduced affinity and with that a diminished biological activity, although the extent may vary depending on the structural context. For allosteric redox switches, both loss-of-function as well as gain-of-function scenarios seem possible with a variable modulation of biological function. In support of this proposal, the available biochemical data for key redox-sensitive proteins with identified NOS/SONOS redox switches indeed indicate a loss of function for proteins with catalytic lysines or cysteines as in case of e.g. DNA repair enzyme OGG1 (Schiff-base lysine) [22] or ubiquitin E2 ligases (catalytic cysteine) [23] under oxidative stress conditions (reaction with H_2O_2). For numerous other cases, it has been established that either reducing conditions are required for full biological activity, or that oxidizing conditions deteriorate protein activity [9, 24-26]. In case of galectin-1, which possesses an allosteric SONOS switch, it was established that the protein exerts different biological functions under oxidizing and reducing conditions and that

binding of effectors requires the reduced state [27,28]. For the human protein, the two corresponding cysteines engaged in forming the SONOS bridge in the *R. norvegicus* ortholog (Fig. 2h) were identified as the redox switch site and suggested to form a disulfide although the latter could not be directly demonstrated [28]. The potential role of NOS redox switches in regulating DNA binding might provide a novel mechanism for the well established redox-dependent action of many transcription factors [8,29]. A putative regulatory role of the detected NOS/SONOS redox switches is further supported by the high degree of conservation of the lysine-cysteine pairs in the protein orthologues (either across different domains of life or in clades of related organisms) despite the fact that in many proteins only one of the two residues has a direct functional role required for biological activity as reported for e.g. OGG1 or rabphilin (SI Tables 3, 4) [30,31].

NOS/SONOS bridges in proteins from pathogens and humans

We further classified the proteins with NOS/SONOS switches regarding their biological function. First, we analysed proteins from human and plant pathogens including viruses, bacteria and parasites (Fig. 7, ED Table 1). In case of pathogenic human viruses, NOS switch-containing proteins with essential roles for all critical phases of the virus life cycle such as infection (adenovirus), replication (SARS-CoV-2) and maturation assembly (cytomegalovirus) were detected. In bacteria and parasites, we identified numerous essential biosynthetic enzymes (amino acid, isoprenoid and polyamine biosynthesis), Na^+ transporters required for ATP biosynthesis, transcription regulators, virulence factors and proteins in the context of pathogen-host interactions. Remarkably, numerous proteins originate from the world's most dangerous pathogens including i.a. SARS-CoV-2 (Covid 19), *Mycobacterium tuberculosis* (tuberculosis), *Vibrio cholerae* (cholera), *Pseudomonas aerigunosa* (pneumonia), *Staphylooccus aureus* (bacterial superinfections), *Legionella pneumophila* (Legionnaires' disease) or *Trypanosoma* species (Chagas disease, African sleeping sickness). NOS bridges were also discovered in major plant pathogens including *Xanthomonas campestris* and *Xanthomonas axonopodis*, the causative agents of "black rot" in cruciferous vegetables and bacterial pustule of soybean [32].

In humans, NOS redox switches are found in different protein families with established roles in oxidative stress response, redox signaling and homeostasis

(Fig. 7, ED Table 2). Major families comprise proteins in DNA repair (excision of oxidized bases, cleavage of protein-DNA crosslinks), in transcription regulation (sensing and binding of DNA, histone writers and erasers), in ribosomal protein translation (translation factors), in protein degradation (ubiquitin E2 ligases, E3 ring ligase), in signaling (various kinases, neurotransmission, inositolphosphate signaling), in the biosynthesis of redox-sensitive cofactors and rare amino acids (Fe-S cluster, S-adenosyl-methionine, selenocysteine) (examples in Fig. 6, ED Fig. 3,5). Also, the enzyme selenophosphate synthetase 1 was identified which is known to be an essential factor of cellular redox homeostasis by regulating the expression levels of e.g. glutaredoxin and glutathione transferase, which protect cells from oxidative stress [33]. Many of the identified human proteins have been inferred in severe diseases including various cancers, Alzheimer's disease, Parkinson's disease, obesity, autoimmune diseases and others (ED Table 2). The discovery of the naturally evolved NOS redox switches may therefore unlock novel therapeutic directions in plenty of disease states by addressing or manipulating the switch site. Prominent examples are e.g. the main protease from SARS-CoV-2 [17,18] or human focal adhesion kinase, which are validated drug targets for treatment of COVID-19 and invasive cancers [34], respectively.

Conclusions

NOS and SONOS redox switches are ubiquitous regulatory elements in proteins that reversibly alter protein function in response to changing redox conditions as e.g. under oxidative stress. They are spontaneously formed without the need of catalysis provided by enzymes or proximal amino acids. The involvement of lysines with direct roles in enzyme catalysis and in binding of enzymatic substrates, nucleic acids and effectors expands the chemical repertoire of organisms to deal with changing redox conditions and constitutes a novel general regulatory principle in biology. Apart from novel directions in medical applications, the identified design principles of naturally evolved NOS/SONOS switches are likely to inspire peptide and protein design [35], in particular the newly found branching SONOS crosslink bears great potential.

References

1.) Schieber, M., & Chandel, N. S. (2014) ROS function in redox signaling and oxidative stress. *Current Biology* 24(10), R453-R462.

2.) Sies, H., & Jones, D. P. (2020) Reactive oxygen species (ROS) as pleiotropic physiological signalling agents. *Nature Reviews Molecular Cell Biology* 21(7), 363-383.

3.) Bazopoulou, D. et al. (2019) Developmental ROS individualizes organismal stress resistance and lifespan. *Nature* 576(7786), 301-305.

4.) Dickinson, B. C., & Chang, C. J. (2011) Chemistry and biology of reactive oxygen species in signaling or stress responses. *Nature Chemical Biology*, 7(8), 504-511.

5.) Sies, H., Berndt, C., & Jones, D. P. (2017) Oxidative stress. *Annual Review of Biochemistry* 86, 715-748.

6.) Reuter, S., Gupta, S. C., Chaturvedi, M. M., & Aggarwal, B. B. (2010) Oxidative stress, inflammation, and cancer: how are they linked? *Free Radical Biology and Medicine* 49(11), 1603-1616.

7.) Paulsen, C. E., & Carroll, K. S. (2013) Cysteine-mediated redox signaling: chemistry, biology, and tools for discovery. *Chemical Reviews* 113(7), 4633-4679.

8.) Choi, H. J., Kim, S. J., Mukhopadhyay, P., Cho, S., Woo, J. R., Storz, G., & Ryu, S. E. (2001) Structural basis of the redox switch in the OxyR transcription factor. *Cell* 105(1), 103-113.

9.) Wensien et al. (2021) A lysine–cysteine redox switch with an NOS bridge regulates enzyme function. *Nature*, in the press, DoI: 10.1038/s41586-021-03513-3

10.) Zhou, P., Tian, F., Lv, F., & Shang, Z. (2009) Geometric characteristics of hydrogen bonds involving sulfur atoms in proteins. *Proteins* 76(1), 151-163.

11.) Neumann, P., & Tittmann, K. (2014) Marvels of enzyme catalysis at true atomic resolution: distortions, bond elongations, hidden flips, protonation states and atom identities. *Current Opinion in Structural Biology* 29, 122-133.

12.) Owen, R. L., Rudiño-Piñera, E., & Garman, E. F. (2006) Experimental determination of the radiation dose limit for cryocooled protein crystals. *Proc. Natl. Acad. Sci. USA* 103(13), 4912-4917.

13.) Wang, J. (2019) Crystallographic identification of spontaneous oxidation intermediates and products of protein sulfhydryl groups. *Protein Science* 28(3), 472-477.

14.) Camby, I., Le Mercier, M., Lefranc, F., & Kiss, R. (2006). Galectin-1: a small protein with major functions. *Glycobiology* 16(11), 137-157.

15.) Davidson, V. L. (2018) Protein-derived cofactors revisited: Empowering amino acid residues with new functions. *Biochemistry* 57(22), 3115-3125.

16.) Ghiladi, R. A., Knudsen, G. M., Medzihradszky, K. F., & de Montellano, P. R. O. (2005). The Met-Tyr-Trp cross-link in Mycobacterium tuberculosis catalase-peroxidase (KatG): autocatalytic formation and effect on enzyme catalysis and spectroscopic properties. *Journal of Biological Chemistry* 280(24), 22651-22663.

17.) Zhang, L. et al. (2020). Crystal structure of SARS-CoV-2 main protease provides a basis for design of improved α-ketoamide inhibitors. *Science* 368(6489), 409-412.

18.) Jin, Z. et al. (2020) Structure of Mpro from SARS-CoV-2 and discovery of its inhibitors. *Nature* 582(7811), 289-293.

19.) Boniecki, M. T., Freibert, S. A., Mühlenhoff, U., Lill, R., & Cygler, M. (2017) Structure and functional dynamics of the mitochondrial Fe/S cluster synthesis complex. *Nature Communications* 8(1), 1-15.

20.) Kang, H. J., Coulibaly, F., Clow, F., Proft, T., & Baker, E. N. (2007) Stabilizing isopeptide bonds revealed in gram-positive bacterial pilus structure. *Science* 318(5856), 1625-1628.

21.) Gross, E., Kastner, D. B., Kaiser, C. A., & Fass, D. (2004) Structure of Ero1p, source of disulfide bonds for oxidative protein folding in the cell. *Cell* 117(5), 601-610.

22.) Bravard, A. et al. (2006). Redox regulation of human OGG1 activity in response to cellular oxidative stress. *Molecular and Cellular Biology* 26(20), 7430-7436.

23.) Obin, M., Shang, F., Gong, X., Handelman, G., Blumberg, J., & Taylor, A. (1998) Redox regulation of ubiquitin-conjugating enzymes: mechanistic insights using the thiol-specific oxidant diamide. *FASEB Journal* 12(7), 561-569.

24.) Veres, Z., Kim, I. Y., Scholz, T. D., & Stadtman, T. C. (1994). Selenophosphate synthetase. Enzyme properties and catalytic reaction. *Journal of Biological Chemistry* 269(14), 10597-10603.

25.) Webby, C. J., Baker, H. M., Lott, J. S., Baker, E. N., & Parker, E. J. (2005). The structure of 3-deoxy-D-arabino-heptulosonate 7-phosphate synthase from Mycobacterium tuberculosis reveals a common catalytic scaffold and ancestry for type I and type II enzymes. *Journal of Molecular Biology* 354(4), 927-939.

26.) Shah, R., Akella, R., Goldsmith, E. J., & Phillips, M. A. (2007) X-ray structure of Paramecium bursaria chlorella virus arginine decarboxylase: insight into the structural basis for substrate specificity. *Biochemistry* 46(10), 2831-2841.

27.) Than, N. G. et al. (2008) Emergence of hormonal and redox regulation of galectin-1 in placental mammals: Implication in maternal–fetal immune tolerance. *Proc. Natl. Acad. Sci. USA* 105(41), 15819-15824.

28.) Guardia, C. M., Caramelo, J. J., Trujillo, M., Méndez-Huergo, S. P., Radi, R., Estrin, D. A., & Rabinovich, G. A. (2014). Structural basis of redox-dependent modulation of galectin-1 dynamics and function. *Glycobiology*, 24(5), 428-441.

29.) Abate, C., Patel, L., Rauscher, F. J., & Curran, T. (1990) Redox regulation of fos and jun DNA-binding activity in vitro. *Science* 249(4973), 1157-1161.

30.) Wang, K., Maayah, M., Sweasy, J. B., & Alnajjar, K. S. (2021) The role of cysteines in the structure and function of OGG1. *Journal of Biological Chemistry* 296, 100093.

31.) Guillén, J. et al. (2013) Structural insights into the Ca^{2+} and PI (4, 5) P2 binding modes of the C2 domains of rabphilin 3A and synaptotagmin 1. *Proc. Natl. Acad. Sci. USA* 110(51), 20503-20508.

32.) da Silva, A. R., et al. (2002) Comparison of the genomes of two Xanthomonas pathogens with differing host specificities. *Nature* 417(6887), 459-463.

33.) Tobe, R. et al. (2016) Selenophosphate synthetase 1 is an essential protein with roles in regulation of redox homoeostasis in mammals. *Biochemical Journal* 473(14), 2141-2154.

34.) McLean, G. W., Carragher, N. O., Avizienyte, E., Evans, J., Brunton, V. G., & Frame, M. C. (2005) The role of focal-adhesion kinase in cancer—a new therapeutic opportunity. *Nature Reviews Cancer* 5(7), 505-515.

35.) Huang, P. S., Boyken, S. E., & Baker, D. (2016) The coming of age of de novo protein design. *Nature* 537(7620), 320-327.

36.) Puvar, K. et al. (2020) Legionella effector MavC targets the Ube2N~ Ub conjugate for noncanonical ubiquitination. *Nature Communications* 11(1), 1-14.

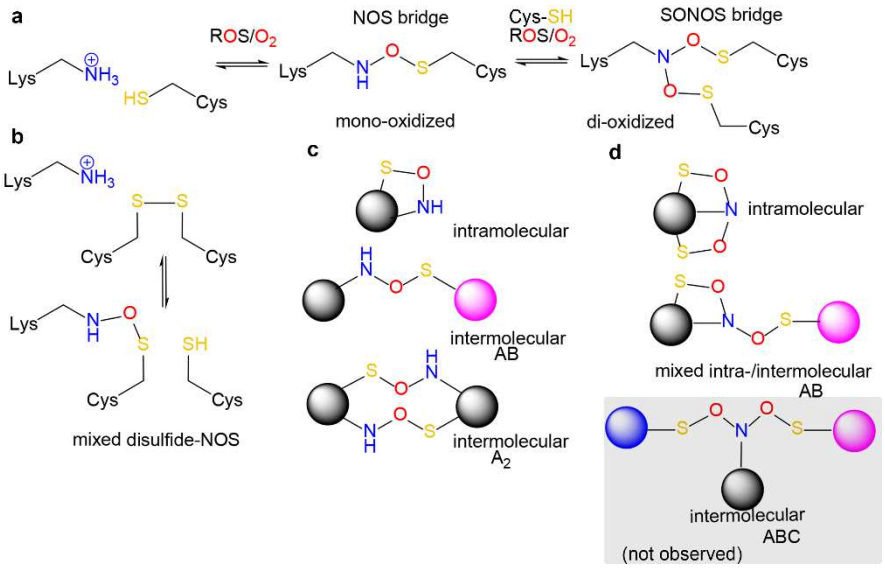

Figure 1. Chemical structures and topologies of NOS and SONOS redox switches in proteins. (**a**) Structures and suggested mechanism of NOS and SONOS redox bridge formation by ROS or O_2 in subsequent oxidation steps. (**b**) Suggested structure of a 'mixed' NOS-disulfide redox switch, in which a disulfide is in equilibrium with an NOS bridge. (**c**) Topologies of NOS bridges showing intramolecular and intermolecular crosslinks as observed in experimentally determined protein structures. (**d**) Topologies of SONOS bridges showing intramolecular and intermolecular crosslinks as observed in experimentally determined protein structures. A SONOS bridge, where the lysine and two cysteines are contributed by three different proteins has not been identified yet.

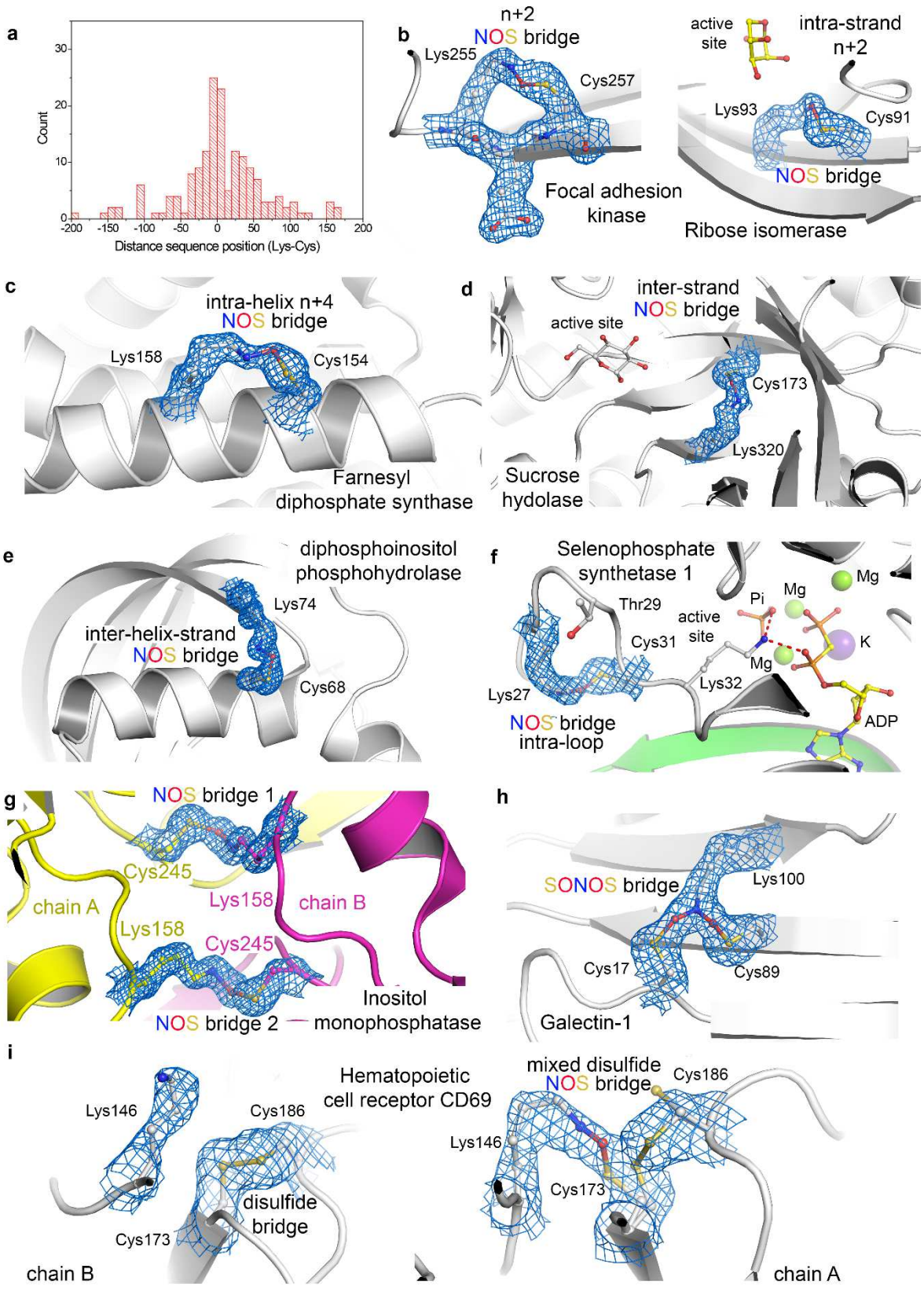

Figure 2. Structural and chemical motifs of NOS bridges in proteins. (**a**) Histogram showing the distribution of detected proteins (non-redundant counts) with NOS bridges in dependence from the distance in sequence between the lysine and cysteine residues. (**b**) Examples for NOS bridges in intra-strand or strand-like motifs with a sequence distance of n+2. Shown are focal adhesion kinase from *Gallus gallus* (pdb code 6CBO) and ribose

isomerase from *Acinetobacter sp.* (pdb code 4Q0P). The 2mFo-DFc electron density maps are shown in blue at a contour level of 1σ. (**c**) Example for an NOS bridge in intra-helix motifs with a sequence distance of n+4. Shown is the farnesyl diphosphate synthase from *Trypanosoma cruzi* (pdb code 6SDP). The 2mFo-DFc electron density map is shown in blue at a contour level of 1σ. (**d**) Example for an NOS bridge in inter-strand (cross-strand) motifs. Shown is the sucrose hydrolase from *Xanthomonas axonopodis* (pdb code 3CZG). The 2mFo-DFc electron density map is shown in blue at a contour level of 1σ. (**e**) Example for an NOS bridge connecting a helix and a neighboring strand showing human diphosphoinositol phosphohydrolase (pdb code 6PCK). The 2mFo-DFc electron density map is shown in blue at a contour level of 1σ. (**f**) Example for an intra-loop NOS bridge showing human selenophosphate synthetase 1 (pdb code 3FD5). The 2mFo-DFc electron density map is shown in blue at a contour level of 1σ. (**g**) Example for an intermolecular NOS double bridge between two chains in a homodimeric assembly. Shown is the inositol monophosphatase from *Medicago truncatula* (pdb code 5EQA). The two chains are colored individually in yellow and magenta, respectively. The 2mFo-DFc electron density map is shown in blue at a contour level of 1σ. (**h**) Example for a SONOS bridge linking a lysine and two cysteines at the same time showing galectin-1 from *Rattus norvegicus* (pdb code 4GA9). The 2mFo-DFc electron density map is shown in blue at a contour level of 1σ. (**e**) Example for a “mixed” NOS-disulfide switch showing the human hematopoietic cell receptor CD69 (pdb code 1E8I). Left panel: chain B with a disulfide bridge between Cys173 and Cys186. Right panel: chain A with an NOS bridge between Lys146 and Cys173 (30% occupancy) and a disulfide bridge between Cys173 and Cys186 (70% occupancy). The 2mFo-DFc electron density maps are shown in blue at a contour level of 1σ.

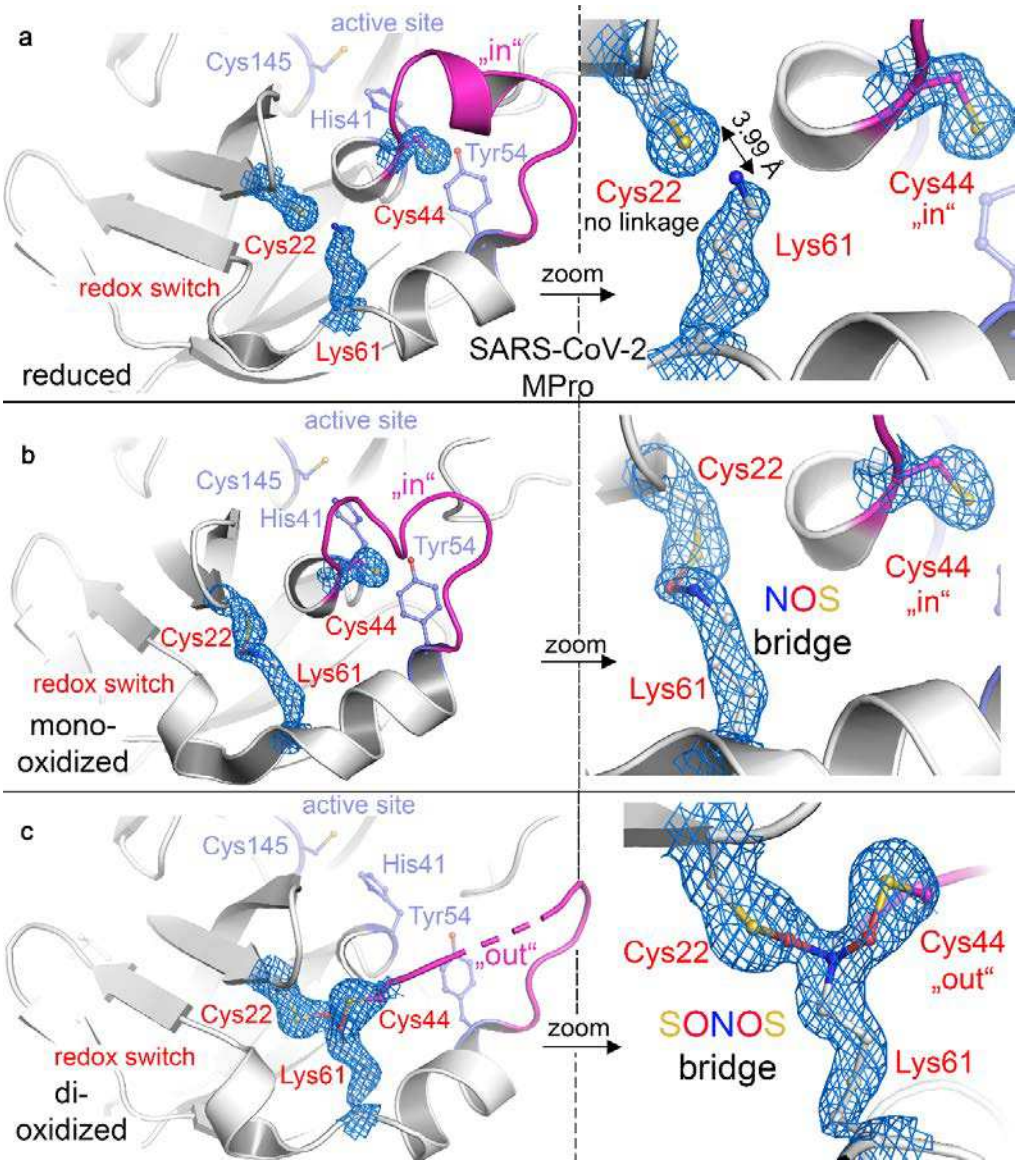

Figure 3. NOS and SONOS bridges in the main protease Mpro from SARS-CoV-2. (**a**) Structure of Mpro in the reduced state (pdb code 7JR3) showing the redox switch at the protein surface formed by residues Cys22, Cys44 and Lys61 (highlighted in red) and the active site with residues Cys145 (catalytic nucleophile), His41 and Tyr54 (highlighted in slate blue). A mobile loop bearing Cys44 is indicated in magenta. Left panel: structural overview. Right panel: close-up of the redox switch site. For residues Cys22, Cys44 and Lys61, the structural models are superposed with the corresponding 2mFo-DFc electron density maps at a contour level of 1σ. Note that residue Cys44 is in the “in-conformation” and interacts with Tyr54. (**b**) Structure of Mpro in the mono-oxidized state with an NOS bridge formed between Cys22 and Lys61 (pdb code 6XMK). Left panel: structural overview. Right panel: close-up of the redox switch site. For residues Cys22, Cys44 and Lys61, the structural models are superposed with the corresponding 2mFo-DFc electron density maps at a contour level of 1σ. Cys44 is found in the “in-conformation”. (**b**) Structure of Mpro in the di-oxidized state with a SONOS bridge formed between Cys22, Lys61 and Cys44 (pdb code 7JR4). Left panel: structural overview. Right panel: close-up of the redox switch site. For residues Cys22, Cys44 and Lys61, the structural models are superposed with the corresponding 2mFo-DFc electron density maps at a contour level of 1σ. Cys44 is found in the “out-conformation”. Competitive refinements (SONOS bridge only, 2 separate NOS bridges, mixture of SONOS and NOS) indicate full occupancy of the SONOS bridge.

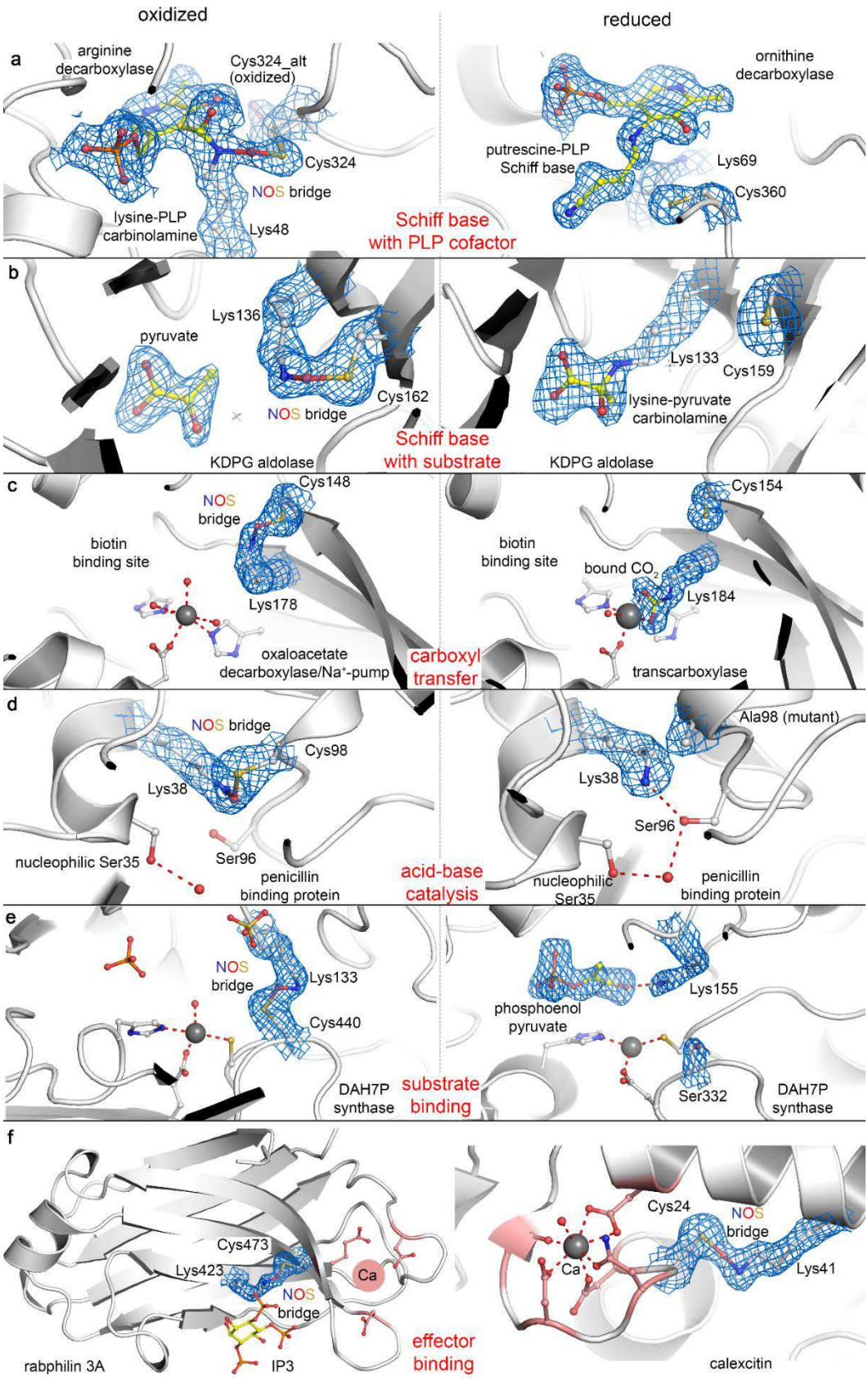

Figure 4. Functional roles of NOS bridge lysines in enzyme catalysis and in binding of enzymatic substrates or effectors. For (a-e), the left panels show the proteins in the oxidized state with the NOS bridge present, while the corresponding right panel shows the same or a closely related protein in the reduced state with the lysine exerting its function. (**a**) Catalytic

lysines forming Schiff-base intermediates in PLP dependent enzymes. Left: Arginine decarboxylase from *Paramecium bursaria* Chlorella Virus (pdb code 2NV9), in which the catalytic Lys48 forms an NOS bridge with Cys324. Right: Ornithine decarboxylase from *Trypanosoma brucei* in covalent complex with product putrescine (pdb code 1F3T). The structural models are superposed with the corresponding 2mFo-DFc electron density maps at 1σ. Note that in the presence of the NOS bridge, the reaction does not proceed beyond the carbinolamine. (**b**) Catalytic lysines forming Schiff-base intermediates with enzymatic substrates. Left: KDPG aldolase from *Oleispira antarctica* in non-covalent complex with substrate pyruvate and with an NOS bridge between Lys136 and Cys162 (pdb code 3VCR). Right: KDPG aldolase from *E. coli* in covalent complex with substrate pyruvate (pdb code 1EUA). The structural models are superposed with the corresponding 2mFo-DFc electron density maps at 1σ. Note that in the presence of the NOS bridge, covalent catalysis is inhibited. (**c**) Catalytic lysines in carboxyl transfer. Left: Oxaloacetate decarboxylase/Na^+ pump from *Vibrio cholerae* with an NOS bridge between Lys178 and Cys148 (pdb code 2NX9). Right: Transcarboxylase 5S subunit from *Propionibacterium freudenreichii* with carboxylated Lys184 (pdb code 1RQB) thought to be an intermediate in CO_2 transfer to biotin. The structural models are superposed with the corresponding 2mFo-DFc electron density maps at 1σ. Note that in the presence of the NOS bridge, catalysis is inhibited. (**d**) Catalytic lysines acting as acid-base catalysts. Left: Penicillin binding protein (transpeptidase) from *Streptomyces sp.* K15 with an NOS bridge between Lys38 and Cys98 (pdb code 1SKF). Right: Penicillin binding protein variant Cys98Ala from *Streptomyces sp.* K15 (pdb code 1ES3). As Lys38 is thought to activate the nucleopilic Ser35 by acid-base catalysis, formation of an NOS bridge under oxidizing conditions is likely to inhibit catalysis. The structural models of residues 38 and 98 are superposed with the corresponding 2mFo-DFc electron density maps at 1σ. (**e**) Lysines with roles in non-covalent binding of enzymatic substrates. Left: DAH7P synthase from *Mycobacterium tuberculosis* (pdb code 3RZI) with an NOS bridge between Lys133 and Cys440. Right: DAH7P synthase from *Listeria monocytogenes* in non-covalent complex with substrate phosphoenolpyruvate (pdb code 3TFC). This enzyme contains a serine (Ser332) at the equivalent position of Cys440 from *M. tuberculosis* DAH7P synthase and can therefore not form an NOS bridge. In the absence of the NOS bridge, the lysine forms a H-bond with the carboxylate moiety of substrate phosphoenolpyruvate. The structural models of key residues and substrate are superposed with the corresponding 2mFo-DFc electron density maps at 1σ. (**f**) Lysines with roles in binding of effectors. Left: Rabphilin 3a from *Rattus norvegicus* in complex with effector inositol trisphosphate (IP3) and with an NOS bridge formed between Lys423 and Cys473 (pdb code 4NP9). Ligand IP3 is weakly occupied with traceable density for the phosphate portions only. Lys423 is directly located at the binding site of IP3. The proximal Ca^{2+} binding site is indicated. Right: Calexcitin from *Loligo pealeii* with an NOS bridge formed between Lys41 and Cys24 proximal to the Ca^{2+} binding site (pdb code 2CCM). The structural models of the NOS bridge-forming lysine and cysteine residues are superposed with the corresponding 2mFo-DFc electron density maps at 1σ.

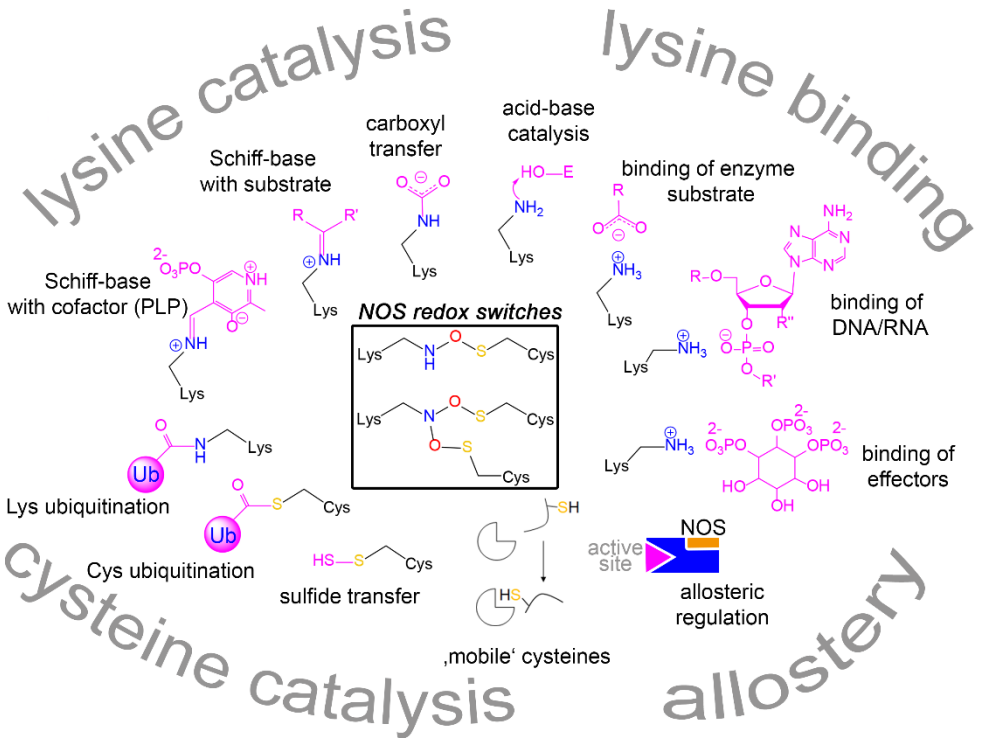

Figure 5. Chemical functions of lysine and cysteine residues forming NOS and SONOS bridges in proteins. Four major functional categories could be identified including i) lysines with catalytic roles in enzyme mechanisms, ii) lysines involved in binding of enzyme substrates, nucleic acids and effectors, iii) cysteines with catalytic roles in enzyme mechanisms and iv) allosteric bridges, which are located remotely relative to the active/functional site. Structures of key reaction intermediates and interaction partners are highlighted. Note that these functions are exerted under reducing conditions that is in the absence of NOS/SONOS bridges. Formation of the NOS or SONOS bridge under oxidizing conditions leads to either a loss-of-function (catalytic lysines, catalytic cysteines), diminished biologial activity (lysine with binding roles) or modulated function (allosteric switches).

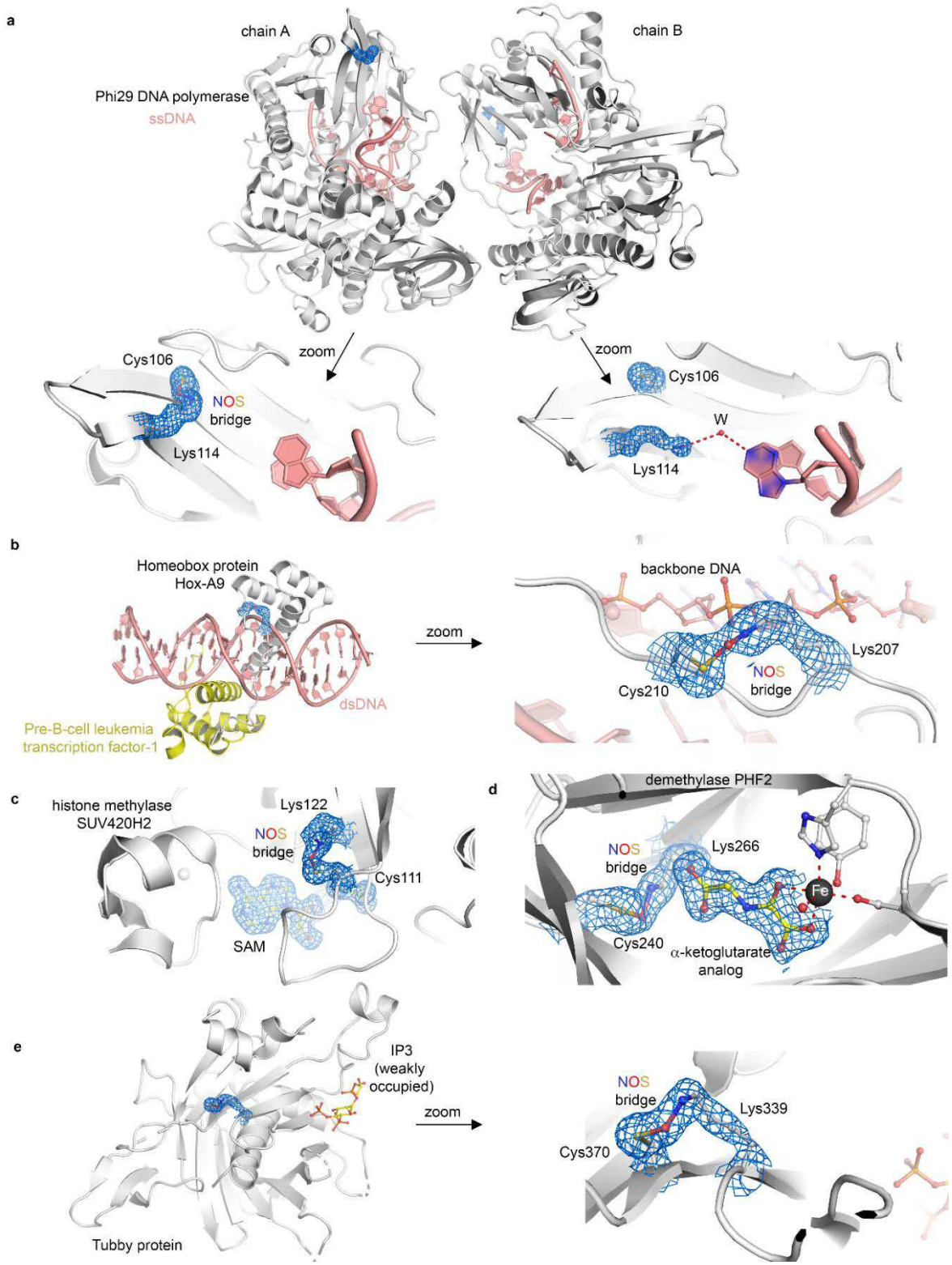

Figure 6. Proteins with NOS bridges inferred in DNA binding and transcription regulation. (**a**) DNA polymerase from Bacillus virus phi29 complexed with single-stranded DNA (pdb code 2PY5). Upper panel: Overall structure showing the two copies (chains a and b) in the asymmetric unit. The single stranded DNA is highlighted in salmon red. Lower panel: Close-up of the NOS redox switch with residues Lys114 and Cys106. Note that in chain A both residues form an NOS bridge (left), which is absent in chain B (right). In the absence of the NOS bridge, Lys 114 forms a H-bond with a DNA base via a water molecule. The structural models of the NOS bridge-forming lysine and cysteine residues are superposed with the

corresponding 2mFo-DFc electron density maps at 1σ. (**b**) Homeobox protein Hox-A9 from *Mus musculus* in complex with human pre-B-cell leukemia transcription factor-1 and double stranded DNA (pdb code 1PUF). Left: Overall structure of the complex. The two proteins are colored individually, the DNA is shown in salmon red. Right: Close-up of the NOS bridge formed between Lys207 and Cys210 of Hox-A9. Note that the NOS bridge is at the binding interface with the backbone of the DNA suggesting that Lys207 in the reduced state interacts with the phosphate groups. The structural models of the NOS bridge-forming lysine and cysteine residues are superposed with the corresponding 2mFo-DFc electron density maps at 1σ. (**c**) Human histone-lysine N-methyltransferase SUV420H2 in complex with substrate S-Adenosyl methionine (SAM) and with an NOS bridge formed between Lys122 and Cys111 (pdb code 3RQ4). Note the proximity of the NOS bridge with respect to the SAM binding locale. The structural models of the NOS bridge-forming lysine and cysteine residues and of the SAM cosubstrate are superposed with the corresponding 2mFo-DFc electron density maps at 1σ. (**d**) Human demethylase PHF2 in complex with an analog of the α-ketoglutarate cofactor and with an NOS bridge formed between Lys266 and Cys240 (pdb code 3PU8). Note the proximity of the NOS bridge with respect to the cofactor binding locale suggesting a direct interaction of Lys266 with the carboxylate moiety of the cofactor. The structural models of the NOS bridge-forming lysine and cysteine residues and of the α-ketoglutarate analog are superposed with the corresponding 2mFo-DFc electron density maps at 1σ. (**e**) Tubby protein from *Mus musculus* in complex with inositol-trisphosphate (pdb code 1I7E). Left: Structural overview highlighting the ligand binding site and the allosteric NOS switch. Right: Close-up of the NOS bridge between Lys339 and Cys370. The structural models of the NOS bridge-forming lysine and cysteine residues are superposed with the corresponding 2mFo-DFc electron density maps at 1σ.

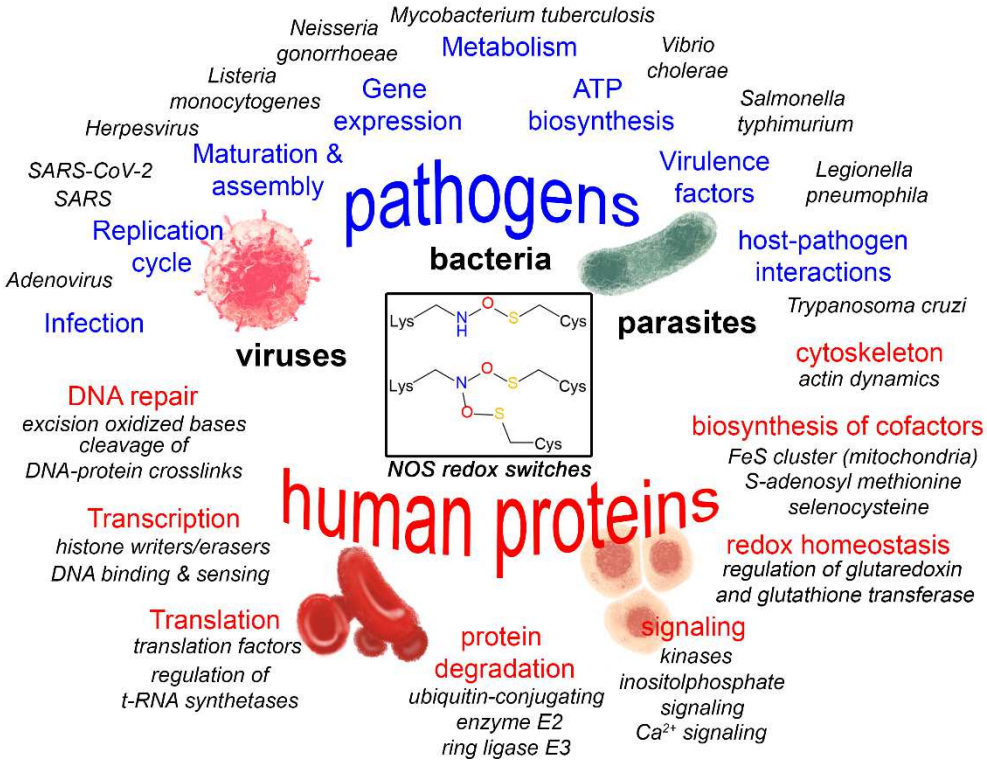

Figure 7. Occurrence and biological functions of proteins containing NOS and SONOS redox switches. Functions of proteins originating from human and plant pathogen are highlighted in blue color, representative examples of relevant species are shown alongside. Cellular functions of human proteins are highlighted in red color, functional subclasses and representative protein families are listed below. Specific information about all proteins regarding origin, biological function, type of NOS/SONOS redox switch, suggested mechanism of the redox switch and potential relevance in disease states is compiled in ED Tables 1 & 2.

Online methods

Experimental Procedures

General information

The protein concentration of *Neisseria gonorrhoeae* transaldolase (*Ng*TAL) was determined by UV/Vis spectroscopy by measuring the absorption at a wavelength of 280 nm and using the molar extinction coefficient (ε_{NgTAL} = 28 420 $M^{-1}cm^{-1}$) determined according to Gill and Hippel [37].

Mutagenesis, protein expression and purification

For expression of *Ng*TAL (UniProtID: Q5F6E9), we used a pET SUMO vector as recently described [9]. Mutant strains were generated by site-directed mutagenesis PCR using the QuikChange site-directed mutagenesis protocol (Stratagene, La Jolla, CA, USA). We used the following primer pair:

*Ng*TAL variant Glu93Gln

Forward: 5'-GTCTGGCACAACATGAAAGCAC-3'

Reverse: 5'-GTGCTTTCATGTTGTGCCAGAC-3'

Expression and purification were carried out as recently reported [9].

Steady-state kinetic analysis

Steady-state kinetic analysis of *Ng*TAL wild-type was carried out using a coupled enzymatic assay that monitors the conversion of ketose donor D-fructose-6-phophate (F6) and aldose acceptor D-erythrose-4-phosphate (E4) into products sedoheptulose-7-phosphate (S7P) and glyceraldehyde-3-phosphate (G3P) at a wavelength of 340 nm [38,39]. Measurements were conducted for both reducing and non-reducing conditions. For measurements under reducing conditions, the protein stock was supplemented in addition with 20 mM dithiothreitol (DTT) resulting in a final concentration of 1 mM DTT in the assay mix. Initial rates were estimated by either linear regression of the absorbance signal over the first 5 s of the measurements, or, in case substrate activation was observed, by using equation 1:

$$A_{340}(t) = A_0 - \Delta ss \cdot t + \frac{\Delta ss - \Delta_0}{k_{obs}} \cdot \left[1 - \exp^{(-k_{obs} \cdot t)}\right] \qquad \text{(eq 1)}$$

with A_0 denoting the starting absorbance at 340 nm, Δss the absorbance change at established steady-state (steady-state rate), Δ_0 the absorbance change at t = 0 (initial rate), and k_{obs} the first-order rate constant of activation for the transition into the fully active enzyme form.

Thus obtained steady-state activities were analyzed using the Michaelis-Menten equation and Hill equation.

Crystallisation, X-ray data collection, processing and model building

*Ng*TAL wild-type and variant Glu93Gln were crystallized and cryoprotected as detailed in [9]. Diffraction data of single protein crystals were collected using synchrotron radiation at beamline P14 of DESY EMBL, Hamburg, Germany, at a wavelength of either 0.9763 Å (*Ng*TAL wild-type, dose series) or 0.689 Å (*Ng*TAL variant Glu93Gln) at 100 K using an EIGER 16M detector. For crystals of *Ng*TAL wild-type, we conducted a series of dose-dependent dataset depositing calibrated doses (0.5-10 MGy in 0.5 MGy increments) per dataset. For data processing the XDS package was used [40]. Subsequent refinement and model building was performed employing PHENIX.REFINE [41] and COOT [42]. Phasing was performed by rigid body refinement using our previously determined *Ng*TAL structure (pdb code 6ZX4) as initial model. The geometry of the structure was validated using MolProbity [43]. Representations of structures were prepared using PyMOL[44]. The Ramachandran statistics are 98.85% in the favoured and 1.15% in the allowed region for 7ODO, 98.85 % and 1.15 % for 7ODP, 98.85% in the favoured and 1.15% in the allowed region for 7ODQ and 98.55% in the favoured and 1.45% in the allowed region for 7OEY.

Computational Methods

We have carried out a series of electronic structure calculations to sample the conformational space and the relative energy of a model system consisting of a single lysine and cysteine residues. The residues were truncated at the *α*-carbon, with the latter represented as a methyl group to reduce the influence of electrostatics in the terminal moieties, closer to what is to expect from a protein backbone. Three different bonding situations were sampled. The first corresponds to a neutral lysine interacting with a cysteine (NHS). The second system considered was a protonated lysine with a cysteine (NHS+). Both cases will build close contacts through hydrogen bonds, either with the lysine as donor (NHS+) or the cysteine (NHS). In the last system we consider the covalently bound residues, with the lysine nitrogen and the cysteine sulfur bonding with an intercalated oxygen atom (NOS).

In a first set of calculations, we studied the dependence of the N-S-distances on the dielectric constant. To this purpose, a representative conformer for each of the systems was optimised in different solvents (vacuum: $\varepsilon = 0.0$, diehtylether: $\varepsilon = 4.2$, acetone: $\varepsilon = 20.5$, methanol: $\varepsilon = 32.6$, 1,2-ethanediol: $\epsilon = 40.2$, dimethylsulfoxide: $\epsilon = 46.8$, water: $\epsilon = 78.4$) [45] using the SMD [46] solvation model. The software package Gaussian16-A.03 [47] was used for the aforementioned calculations, with the B3LYP-D3(BJ)/def2-SVP [48-51] level of theory. A constrained *α*-carbon distance of 10 Å was applied for all the calculations with different solvents. The results are provided in SI Fig. 1. The only difference observed was a smaller difference between the distances observed in the NHS and NHS+ systems. Considering the stable behavior of the N-S-distances in different environments the following calculations were carried out in vacuum for simplicity and for a more straightforward generalisation.

Three different *α*-carbon distances (6, 8 and 10˚A) between lysine and cysteine were applied for the extended sampling runs (the results are provided in ED Figure 1). Initial conformer sampling was carried out using CREST-2.10.2 [52], whereby the conformer optimization was conducted with xTB-6.4.0 [53] using the semiempirical tight-binding based

quantum chemistry method GFN2-xTB [54] with the ”extreme” optimization criteria (E_{conv} = 5 × 10^{-8} Hartree) and the ”NCI” option.

After initial global sampling at the semiempirical level, the structures were refined in two stages at the density functional theory (DFT) level. For NOS, the collected GFN2-xTB conformer structures were further optimized using B3LYP-D3(BJ)/def2-SVP [48-51], again with the use of the Gaussian16-A.03 program package. Conformers with imaginary frequencies were directly abandoned and not used further for optimization or data statistics. For neutral and protonated hydrogen bonded systems (NHS and NHS+) the conformers were additionally filtered to guarantee the existence of hydrogen bonds and, thereby, afford the closest contacts possible. As criteria a distance shorter than 2.5 Å between the hydrogen (H) and the hydrogen acceptor (A) and an angle ADH (D: hydrogen donor) smaller than 30° were taken. Determination of the hydrogen atom for the building of the hydrogen bond follows the shortest distance among the potential hydrogen bonds between the amine and thiol residues.
The conformations obtained from B3LYP-D3(BJ)/def2-SVP were in a further stage sorted according to their electronic energies from low to high. If the energy difference between two conformations was larger than 0.1 kcal/mol and the root-mean-square difference (RMSD) for the superimposed structures larger than 0.125 Å [55], the two conformations were considered to be unique and subject to further calculations. From this pool of structures, we considered the lowest-lying conformers (up to 2 kcal/mol in difference to the global minimum) and carried out further optimizations at the B3LYP-D3(BJ)/def2-TZVPP level of theory. For both NHS and NHD+ systems the additional filter process to verify the existence of hydrogen bonds was again applied. The results of the first (B3LYP-D3(BJ)/def2-SVP) and the second stage (B3LYP-D3(BJ)/def2-TZVPP) of optimizations were used and displayed in ED Figure 1. An overview of different geometric values and their correlation for the NOS bond is provided in SI Fig. 2.

In a further set of calculations, we investigated what could be the lowest energy conformer for both NHS and NHS+ bearing a N-S distance of 2.7 Å. By comparing the results of this sampling, we were able to assess the energy penalty associated with bringing the two residues in such a close vicinity without any covalent bond formation. This involved two further sampling rounds with the *α*-carbon distances set to 8 Å. The latter choice was considered as non-critical, given that the relative energetic and geometry information for the different bonding situations did not change dramatically upon variation of said parameter. Each sampling run was performed following the same steps as before, but with an added constraint to the N-S-distance of 2.7 Å. No additional filter process for hydrogen bonds was applied. RMSD criteria were also not applied since we were not interested in a distribution, but simply the most energetically stable geometry. The energies of the lowest conformers (“global” minima) were compared for the runs with and without the distance constraint. This resulted in an energy gap of 4.3 kcal/mol (SI Fig. 3). The thermochemical calculations for formation of the SONOS bridge are exemplified shown for the SARS-CoV-2- main protease Mpro (SI Fig. 4), which showcase a putative pathway for two subsequent oxidation steps.

Search of the Protein Data Bank for potential NOS or SONOS bridges

On December 2nd 2020, we searched all deposites structures at the pdb (www.rcsb.org) with a resolution of 2 Å or better (65,327 out of ~170,000 structures) for potential NOS or SONOS bridges, using the program NCONT of the CCP4 suite [56]. In view of the quantum

chemically calculated N-S interatomic distance of 2.6-2.7 Å for NOS bridges, we defined thresholds of 3.00 Å as upper limit and 2.45 Å as lower limit for the search. As non-covalent hydrogen-bond interactions between lysines and cysteines exhibit interatomic distances of >3.2 Å, we considered a cut-off at 3 Å to be a robust discriminator between covalent and non-covalent Cys-Lys interactions. A total of 285 pdb entries with ~400 potential NOS/SONOS bridges were identified, for 266 of these the corresponding structure factors were deposited. We examined all entries manually and inspected the potential NOS/SONOS redox switch sites. In case the electron density maps indicated the presence of a covalent crosslink between the lysine N atom and the cysteine S atom, we rebuilt the structural model with an NOS/SONOS bridge and compared the obtained models and electron density maps with those calculated for structures with a non-covalent interaction between the lysine and cysteine side chains. Model building was carried out using COOT [42], and refinements were done with PHENIX.REFINE [41].

Analysis of sequence conservation

The analysis of sequence conservation of lysine and cysteine residues forming NOS or SONOS bridges was performed for the 1,000 closest related protein sequences obtained using BLASTP [57] for the respective protein of interest. Alignment was performed using MAFFT [58].

References

37.) Gill, S. C., & Von Hippel, P. H. (1989) Calculation of protein extinction coefficients from amino acid sequence data. *Analytical Biochemistry* 182(2), 319-326.

38.) Tsolas, O and L Joris (1975) Transaldolase. *Methods in Enzymology* 42, 290–297.

39.) Sautner, V. et al. (2015) Converting Transaldolase into Aldolase through Swapping of the Multifunctional Acid–Base Catalyst: Common and Divergent Catalytic Principles in F6P Aldolase and Transaldolase. *Biochemistry* 54 (29), 4475–4486.

40.) Kabsch, W. (2010) XDS. *Acta Cryst Sect D Biol Crystallography* 66, 125-132.

41.) Adams, Paul D., et al. (2010) PHENIX: a comprehensive Python-based system for macromolecular structure solution *Acta Cryst Sect D Biol Crystallography* 66, 213-221.

42.) Emsley, P., Lohkamp, B. (2010) Features and development of Coot. *Acta Crystallogr. D. Biol. Crystallogr.* 66, 486–501.

43.) Williams et al. (2018) MolProbity: More and better reference data for improved all-atom structure validation. *Protein Sci.* 27, 293-315.

44.) Schrödinger, L. L. C. (2015) “The PyMOL Molecular Graphics System, Version 1.8.”

45.) https://gaussian.com/scrf/, updated on: 07 April 2021.

46.) Marenich, A. V., Cramer, C. J., and Truhlar, D. G. (2009) Universal solvation model based on solute electron density and on a continuum model of the solvent defined by the bulk dielectric constant and atomic surface tensions. *The Journal of Physical Chemistry B* 113(18), 6378–6396.

47.) Gaussian 16, Revision C.01, Frisch, M. J., Trucks, G. W., Schlegel, H. B., Scuseria, G. E., Robb, M. A., Cheeseman, J. R., Scalmani, G., Barone, V., Petersson, G. A., Nakatsuji, H., Li, X., Caricato, M., Marenich, A. V., Bloino, J., Janesko, B. G., Gomperts, R., Mennucci, B., Hratchian, H. P., Ortiz, J. V., Izmaylov, A. F., Sonnenberg, J. L., Williams-Young, D., Ding, F., Lipparini, F., Egidi, F., Goings, J., Peng, B., Petrone, A., Henderson, T., Ranasinghe, D., Zakrzewski, V. G., Gao, J., Rega, N., Zheng, G., Liang, W., Hada, M., Ehara, M., Toyota, K., Fukuda, R., Hasegawa, J., Ishida, M., Nakajima, T., Honda, Y., Kitao, O., Nakai, H., Vreven, T., Throssell, K., Montgomery, J. A., Jr., Peralta, J. E., Ogliaro, F., Bearpark, M. J., Heyd, J. J., Brothers, E. N., Kudin, K. N., Staroverov, V. N., Keith, T. A., Kobayashi, R., Normand, J., Raghavachari, K., Rendell, A. P., Burant, J. C., Iyengar, S. S., Tomasi, J., Cossi, M., Millam, J. M., Klene, M., Adamo, C., Cammi, R., Ochterski, J. W., Martin, R. L., Morokuma, K., Farkas, O., Foresman, J. B., Fox, D. J. Gaussian, Inc., Wallingford CT, 2016.

48.) Becke, A. D. (1993) Density-functional thermochemistry. III. The role of exact exchange. *J. Chem. Phys.* 98(7), 5648–5652.

49.) Grimme, S., Antony, J., Ehrlich, S., and Krieg, H. (2010) A consistent and accurate ab initio parametrization of density functional dispersion correction (DFT-D) for the 94 elements h-pu. *The Journal of Chemical Physics*, 132(15), 154104

50.) Grimme, S., Ehrlich, & S., Goerigk, L. (2011) Effect of the damping function in dispersion corrected density functional theory. *J. Comput. Chem.* 32(7), 1456-1465.

51.) Weigend, F., and Ahlrichs, R. (2005) Balanced basis sets of split valence, triple zeta valence and quadruple zeta valence quality for h to rn: Design and assessment of accuracy. *Physical Chemistry Chemical Physics*, 7(18), 3297– 3305.

52.) Grimme, S. (2019) Exploration of chemical compound, conformer, and reaction space with meta-dynamics simulations based on tight-binding quantum chemical calculations. *Journal of Chemical Theory and Computation*, 15(5), 2847–2862.

53.) Bannwarth, C., Caldeweyher, E., Ehlert, S., Hansen, A., Pracht, P., Seibert, J., Spicher, S., and Grimme, S. (2021) Extended tight-binding quantum chemistry methods. *WIREs Computational Molecular Science*, 11(2), e1493, 2021.

54.) Bannwarth, C., Ehlert, S., and Grimme, S. (2019) Gfn2xtb—an accurate and broadly parametrized self-consistent tight-binding quantum chemical method with multipole electrostatics and densitydependent dispersion contributions. *Journal of Chemical Theory and Computation*, 15(3), 1652–1671.

55.) Pracht, P., Bohle, F., and Grimme, S. (2020) Automated exploration of the low-energy chemical space with fast quantum chemical methods. *Phys. Chem. Chem. Phys.*, 22, 7169–7192.

56.) Winn, M. D. et al. (2011). Overview of the CCP4 suite and current developments. *Acta Crystallographica Section D: Biological Crystallography* 67(4), 235-242.

57.) Myers, W. G. W. M. E., Altschul, S. F., & Lipman, D. J. (1990) Basic local alignment search tool. *J. Mol. Biol.* 215(3), 403-10.

58.) Katoh, K., Misawa, K., Kuma, K. I., & Miyata, T. (2002) MAFFT: a novel method for rapid multiple sequence alignment based on fast Fourier transform. *Nucleic Acids Research* 30(14), 3059-3066.

Acknowledgements

This study was supported by the Max-Planck Society and the DFG-funded Göttingen Graduate Center for Neurosciences, Biophysics, and Molecular Biosciences GGNB. We acknowledge access to beamline P14 at DESY/EMBL Hamburg, Germany and thank Gleb Bourenkov and Thomas Schneider for local support. We thank Tom Curran, Brenda Schulman, Sonja Lorenz, Rolf Hilgenfeld, Roland Lill, Reinhard Jahn, Nils Brose, Arwen Pearson, Deborah Fass, Holger Stark, Manuel Alcarazo, Ralph Golbik, Hennig Urlaub, Ute Curth and Jared Rutter for discussion.

Data availability

The refined structural protein models and corresponding structure-factor amplitudes are deposited under PDB accession codes 7OEY (*Ng*TAL variant Glu93Gln oxidized), 7ODO (*Ng*TAL wild-type oxidized, 0.5 MGy dose), 7ODP (*Ng*TAL wild-type oxidized, 5 MGy dose), 7ODQ (*Ng*TAL wild-type oxidized, 10 MGy dose). All structures cited in this publication are available under their respective PDB accession codes. All other data are available on request.

Competing interests

F.R.v.P., M.W., L.-M.F., J.U., R.A.M., and K.T. have filed a European patent application (application number EP21164101.4) for regulating protein activities by targeting the NOS or SONOS redox switches.

Supplementary Files

This is a list of supplementary files associated with this preprint. Click to download.

- EDcompiledTittmann2021NCB.pdf
- SIData1.xlsx
- SIfinaltittmann2021.pdf